Numerical feedback controller design for PDE systems using model reduction: techniques and case studies

F. LEIBFRITZ * *and S. VOLKWEIN* †

1 Introduction

Recently the application of reduced–order models to optimal control problems for partial differential equations (PDEs) has received an increasing amount of attention. The reduced–order approach is based on projecting the dynamical system onto subspaces consisting of basis elements that contain characteristics of the expected solution. This is in contrast to, e.g., finite element techniques, where the elements of the subspaces are uncorrelated to the physical properties of the system that they approximate. One reduced basis method is proper orthogonal decomposition (POD). It has been successfully used in a variety of fields, see, for instance, in [9, 22] for detailed reference lists.

Output feedback controller synthesis for linear control systems that meet desired performance and/or robustness specifications is an attractive model–based control design tool and has been an active research area of the control community for several decades (see, e.g., [7, 30]). It is not always possible to have full access to the state of the control system and a controller based on the measurements has to be used. Output feedback synthesis without additional complexity constraints yields in general a controller order equal to n_x the dimension of the dynamical

*University of Trier, FB–IV Department of Mathematics, D–54286 Trier, Germany. (leibfr@uni-trier.de)

†University of Graz, Institute of Mathematics and Scientific Computing, Graz, Austria. (stefan.volkwein@uni-graz.at)

system. The computation of the controller action becomes more expensive with increasing controller dimension. This is one reason why full order synthesis control has not been widely used in industry. Recently, linear matrix inequalities (LMIs) have attained much attention in control engineering [4], since many control problems can be formulated in terms of LMIs and thus solved via convex programming approaches. However, the resulting controllers are state feedback or of order n_x equal to the plant. For example, difficulties arise if we want to design a static output feedback (SOF) control law. In this case, the control problems consist of finding a SOF controller which minimizes a performance measure subject to stability and/or robustness constraints. It is known that they can be rewritten to non–convex matrix optimization problems (see [10, 12, 18]). Notice that in [17] the first author extends these matrix optimization problems to nonlinear semidefinite programs (NSDPs) by including explicitly the stability condition (modeled by two matrix inequalities) into the problem formulation. Finding a numerical solution to the non–convex NSDP is a difficult task, particularly, if the dimension of the NSDP is large. Usually this will be the case if the control system dynamics are given by a partial differential equation. Then, the dimension of the discretized counterpart can be very large and the computation of an output feedback controller may be impossible. In particular, the SOF case requires the solution of a large scale NSDP with several million variables, which is usually not solvable. This is one of our main motivations for considering the SOF problem for PDE constrained control problems in combination with the POD method for deriving a low dimensional control system and the interior point trust region (IPCTR) algorithm for solving the corresponding low dimensional NSDP. The SOF control law can be constructed from the solution of the low dimensional NSDP. In our numerical examples, we will demonstrate that this SOF can be used for controlling the large dimensional PDE system. In particular, we illustrate that the choice of the POD norms as well as the POD snapshots can improve the stability properties of the computed SOF gain.

The paper is organized in the following manner: In Section 2 we review the POD method and recall some pre–requisites needed for the numerical experiments. The discussion of static output feedback control design problems for finite dimensional systems and a sketch of IPCTR is contained briefly in Section 3. Numerical tests are carried out in Section 4 and in the last section we draw some conclusions.

`Notation:` Throughout this paper, $\mathcal{S}^n$ denotes the linear space of real symmetric $n \times n$ matrices. In the space of real $m \times n$ matrices we define the inner product by $\langle M, Z\rangle = Tr(M^T Z)$ for $M, Z \in \mathbb{R}^{m\times n}$, where $Tr(\cdot)$ is the trace operator, and $\|\cdot\|$ denotes the Frobenius norm given by $\|M\| = \langle M, M\rangle^{1/2}$, while other norms and inner products will be specified. For a matrix $M \in \mathcal{S}^n$ we use the notation $M \succ 0$ or $M \succeq 0$ if it is positive definite or positive semidefinite, respectively. For a twice differentiable mapping $G : \mathcal{U} \to \mathcal{W}$ ($\mathcal{U}$, $\mathcal{W}$ Banach spaces) we denote by G_U, G_{UU} the first and second partial derivatives of G with respect to U. Moreover, $G_U(\cdot)H$ is used when a linear operator $G_U(\cdot)$ is applied to an element $H \in \mathcal{U}$. Furthermore, $G^*_U(\cdot)$ denotes the adjoint of $G_U(\cdot)$ and $\mathcal{L}(\mathcal{U}, \mathcal{V})$ refers to the space of linear, bounded operators endowed with the common norm.

2 Proper orthogonal decomposition (POD)

POD is a method to derive reduced–order models for dynamical systems. In this section we introduce the POD method for nonlinear dynamical systems and propose the numerical realization of POD. Let us consider the following semi–linear initial value problem

$$\begin{aligned} \dot{x}(t) + \mathcal{A}x(t) &= f(t, x(t)) \quad \text{for } t \in (0, T), \\ x(0) &= x_\circ, \end{aligned} \tag{1}$$

where $-\mathcal{A}$ is the infinitesimal generator of a C_0-semigroup $S(t)$, $t > 0$, on a Hilbert space Ξ, $x_\circ \in \Xi$ and $f : [0, T] \times \Xi \to \Xi$ is continuous in t and uniformly Lipschitz–continuous on Ξ for every t. Problem (1) has a unique mild solution $x \in C([0, T]; \Xi)$ given implicitly by the integral representation

$$x(t) = S(t)x_\circ + \int_0^t S(t - s)f(s, x(s))\,\mathrm{d}s \quad \text{for } t \in (0, T), \tag{2}$$

see, for instance, [24, p. 184]. If, in addition, f is continuously differentiable, then the mild solution (2) with $x_\circ \in D(\mathcal{A}) = \{\varphi \in \Xi : \mathcal{A}\varphi \in \Xi\}$ is also a classical solution, i.e., $x \in C^1([0, T]; \Xi)$ holds and x satisfies (1) for all $t \in [0, T]$, see, e.g., [24, p. 187].

Let $\mathcal{U}$ and $\mathcal{W}$ be real separable Hilbert spaces and suppose that $\mathcal{U}$ is dense in $\mathcal{W}$ with compact embedding. Throughout we assume that Ξ denote either the space $\mathcal{U}$ or $\mathcal{W}$ and that x denotes the unique solution to (1) with $x \in C^1([0, T]; \Xi)$. For given $n \in \mathbb{N}$ let

$$0 \le t_1 < t_2 < \ldots < t_n \le T$$

denote a grid in the interval $[0, T]$ and define

$$w_j = \begin{cases} x(t_j) & \text{for } j = 1, \ldots, n, \\ \dot{x}(t_{j-n}) & \text{for } j = n + 1, \ldots, 2n. \end{cases} \tag{3}$$

Setting $n_1 = n$ and $n_2 = 2n$ we introduce two different linear spaces by

$$\mathcal{V}_1 = \text{span}\,\{w_1, \ldots, w_{n_1}\} \quad \text{and} \quad \mathcal{V}_2 = \text{span}\,\{w_1, \ldots, w_{n_2}\}$$

We refer to $\mathcal{V}_1$ as the ensemble consisting of the so-called snapshots $\{x(t_j)\}_{j=1}^n$, compare [25], whereas $\mathcal{V}_2 \supseteq \mathcal{V}_1$ also includes the time derivatives $\dot{x}(t)$ at $t = t_j$ for $1 \le j \le n$. By (1) and (3), we have

$$w_{n+j} = \dot{x}(t_j) = \mathcal{G}(t, x_j), \quad j = 1, \ldots, n,$$

with $\mathcal{G}(t, x) = -\mathcal{A}x + f(t, x)$ for $(t, x) \in [0, T] \times \Xi$. Since we are interested in building up a reduced–order model for (1), we want to utilize snapshots that are best suited for reconstruction of the nonlinear dynamics $\mathcal{G}(t, x)$. Therefore, the set $\mathcal{V}_2$ contains, in addition to the set $\mathcal{V}_1$, information about the spatial derivatives and nonlinearities in the dynamical system, compare, e.g., [1, 15]. It follows that $\mathcal{V}_k \subset \Xi$ by construction, $k = 1$ or 2.

Let $\{\psi_i\}_{i=1}^{d_k}$ denote an orthonormal basis for $\mathcal{V}_k$ with $d_k = \dim \mathcal{V}_k$ for $k = 1$ or 2. Then each member of the ensemble can be expressed as

$$w_j = \sum_{k=1}^{d_k} \langle w_j, \psi_i \rangle_\Xi \psi_i \quad \text{for } j = 1, \ldots, n_i. \tag{4}$$

For $k = 1$ or 2 the method of POD consists in choosing an orthonormal basis such that for every $\ell \in \{1, \ldots, d_k\}$ the mean square error between the elements w_j, $1 \le j \le n_k$, and the corresponding ℓ-th partial sum of (4) is minimized on average:

$$\begin{aligned} &\min \ \frac{1}{n_k} \sum_{j=1}^{n_k} \Big\| w_j - \sum_{i=1}^{\ell} \langle w_j, \psi_i \rangle_\Xi \psi_i \Big\|_\Xi^2 \\ &\text{subject to } \langle \psi_i, \psi_j \rangle_\Xi = \delta_{ij} \quad \text{for } 1 \le i \le \ell,\ 1 \le j \le i. \end{aligned} \tag{5}$$

A solution $\{\psi_i\}_{i=1}^{\ell}$ to (5) is called *POD basis of rank* ℓ. The subspace spanned by the first ℓ POD basis functions is denoted by $\mathcal{V}^\ell$, i.e.,

$$\mathcal{V}^\ell = \text{span}\, \{\psi_1, \ldots, \psi_\ell\}. \tag{6}$$

Utilizing a Lagrangian framework the solution of (5) is characterized by the necessary optimality condition, which can be written as an eigenvalue problem (see, e.g., [11, pp. 88-91] and [27, Section 2]). For that purpose we introduce the positive semidefinite and symmetric matrix $\mathcal{K}_k \in \mathbb{R}^{n_k \times n_k}$, $k = 1$ or 2, with elements

$$\big(\mathcal{K}_k\big)_{ij} = \frac{1}{n_k} \langle w_j, w_i \rangle_\Xi$$

The matrix $\mathcal{K}_k$ is often called a *correlation matrix.* Let $\lambda_1 \ge \lambda_2 \ge \ldots \ge \lambda_{d_k} > 0$ and $v_1, \ldots, v_{d_k} \in \mathbb{R}^{n_k}$ denote the d_k positive eigenvalues of $\mathcal{K}_k$ and the corresponding eigenvectors, respectively, i.e., we have

$$\mathcal{K}_k v_i = \lambda_i v_i, \quad i = 1, \ldots, d_k. \tag{7}$$

Then the POD basis functions are given by

$$\psi_i = \frac{1}{n_k \sqrt{\lambda_i}} \sum_{j=1}^{n} v_i^j w_j \quad \text{for } i = 1, \ldots, \ell, \tag{8}$$

where v_i^j stands for the j-th component of the eigenvector v_i.

Remark 1. POD is closely related to the singular value decomposition. This fact is very useful for implementation issues, in particular, for the computation of the POD basis functions ψ_i as well as of the corresponding eigenvalues λ_i, $1 \le i \le \ell$. The finite–dimensional case was studied in [14], whereas the infinite–dimensional case was analyzed in [22, 28]. $\diamond$

If the POD basis $\{\psi_i\}_{i=1}^{\ell}$ is determined, e.g., by solving (7) and using (8), we obtain the following value for the cost functional in (5):

$$\frac{1}{n_k}\sum_{j=1}^{n_k}\Big\|w_j-\sum_{i=1}^{\ell}\langle w_j,\psi_i\rangle_\Xi\psi_i\Big\|_\Xi^2=\sum_{\ell+1}^{d_k}\lambda_i,$$

see [27, Section 2], for instance. Thus, if the decay of the eigenvalues λ_i is very rapid, the term $\sum_{\ell+1}^{d_k}\lambda_i$ is small, even for a small value of ℓ. In this case only a few POD basis functions represent the ensemble $\mathcal{V}_1$ or $\mathcal{V}_2$ in a sufficient manner. One heuristic to choose the number ℓ of POD basis functions is

$$\mathcal{E}_k(\ell)=\frac{\sum_{i=1}^{\ell}\lambda_i}{\sum_{i=1}^{d_k}\lambda_i}\cdot 100\ \%\approx 99\ \%,\quad k\in\{1,2\}.$$

Obviously, we have $\mathcal{E}_k(d_k)=100\ \%$.

In Section 4 we compare the performance of POD model reduction by utilizing either $\mathcal{V}_1$ or $\mathcal{V}_2$ and by taking either $\Xi=\mathcal{U}$ or $\Xi=\mathcal{W}$ with the choices $\mathcal{W}=L^2(\Omega)$ and $\mathcal{U}=H^1(\Omega)$.

3 Numerical design of SOF control laws

We present a numerical strategy for the computation of a linear SOF control law for discretized PDE control systems. In example, a finite difference or finite element discretization of a PDE control problem yields a finite dimensional control system of the following general form:

$$\begin{aligned} E\dot{x}(t) &= (A+\delta A)x(t)+G(x(t))+B_1\tilde{w}(t)+Bu(t),\quad x(0)=x_\circ,\\ z(t) &= C_1x(t)+D_1u(t),\quad y(t)=Cx(t), \end{aligned}\tag{9}$$

where $x\in\mathbb{R}^{n_x}$ is the approximation of the state, $u\in\mathbb{R}^{n_u}$ is the control input, $y\in\mathbb{R}^{n_y}$ denotes the measurements, $\tilde{w}\in\mathbb{R}^{n_w}$ is a disturbance input, $z\in\mathbb{R}^{n_z}$ the regulated output, $E\in\mathbb{R}^{n_x\times n_x}$ is a regular diagonal matrix and $A\in\mathbb{R}^{n_x\times n_x}$, $B\in\mathbb{R}^{n_x\times n_u}$, $B_1\in\mathbb{R}^{n_x\times n_w}$, $C\in\mathbb{R}^{n_y\times n_x}$, $C_1=\sqrt{0.5c_1}\,[I_{n_x}\ \ 0_{n_u\times n_x}]^T$, $D_1=\sqrt{0.5d_1}\,[0_{n_x\times n_u}\ \ I_{n_u}]^T$ with $c_1,d_1\in\mathbb{R}$ are given positive scalars. If $\delta A\equiv 0$ the system matrix A is not affected by a perturbation, and, if $G(x(t))\equiv 0$, the system is linear. Depending on the corresponding PDE model, we get linear or nonlinear control systems which we want to control by a linear SOF control law of the form

$$u(t)=Fy(t),\quad F\in\mathbb{R}^{n_u\times n_y}.\tag{10}$$

If we neglect the nonlinear term $G(x(t))$ in (9) and substitute this linear SOF control into the state space plant (9), then we obtain the following linear closed loop system:

$$\dot{x}(t)=A(F)x(t)+B(F)\tilde{w}(t),\quad z(t)=C(F)x(t),\tag{11}$$

where $A(F):=E^{-1}(A+\delta A+BFC)$, $B(F):=E^{-1}B_1$, $C(F):=C_1+D_1FC$ are the closed loop operators, respectively.

SOF design and NSDP formulation

One of the most basic static output feedback design problem is the SOF–$\mathcal{H}_2$ problem (see [17, 26]): *Find a SOF gain F such that the closed loop matrix $A(F)$ is Hurwitz and the $\mathcal{H}_2$ norm of* (11) *is minimal.* It is well known that this problem can be rewritten to the following $\mathcal{H}_2$–NSDP, see, e.g. [19, 21, 22],

$$\min \ \ \mathrm{Tr}(LB_1B_1^T) \ \text{ s. t. } \quad \begin{array}{l} A(F)^TV + VA(F) + I = 0, \ V \succ 0, \\ A(F)^TL + LA(F) + C(F)^TC(F) = 0, \end{array} \tag{12}$$

where $L, V \in \mathcal{S}^{n_x}$. Note, (12) is bilinear in L, V, F and quadratic in F, hence non–convex in the free variables. Therefore different local minima might occur and any suitable NSDP solver usually determines a local solution of the matrix optimization problem. A more attractive and realistic model–based control design tool is the mixed $\mathcal{H}_2/\mathcal{H}_\infty$ synthesis. It allows incorporation of model uncertainties in the control design. The SOF–$\mathcal{H}_2/\mathcal{H}_\infty$ problem can be formally stated in the following term, see, e. g. [3, 18, 13]: *For a given scalar $\gamma > 0$ find a SOF matrix F such that $A(F)$ is Hurwitz, the $\mathcal{H}_\infty$ norm of* (11) *is less than γ and the $\mathcal{H}_2$ norm of* (11) *is minimal.* For computing the SOF–$\mathcal{H}_2/\mathcal{H}_\infty$ gain F, we consider the following known $\mathcal{H}_2/\mathcal{H}_\infty$–NSDP version, see, e.g. [19, 22]:

$$\begin{array}{l} \min \ \mathrm{Tr}(LB_1B_1^T) \ \text{ s. t. } \ A(F)^TL + LA(F) + C(F)^TC(F) + \frac{1}{\gamma^2}LB_1B_1^TL = 0, \\ \qquad (A(F) + \frac{1}{\gamma^2}B_1B_1^TL)^TV + V(A(F) + \frac{1}{\gamma^2}B_1B_1^TL) + I = 0, \ \ V \succ 0. \end{array} \tag{13}$$

Due to the bilinearity of the free matrix variables it is a non–convex NSDP, too.

The NSDP Algorithm – Sketch of IPCTR

Our goal is to solve the NSDPs defined in the previous paragraph by IPCTR originally developed in [20] and augmented in [22] for solving NSDPs of the form

$$\min \quad J(X) \quad \text{s. t.} \quad H(X) = 0, \quad G(X) = 0, \quad Y(X) \succeq 0, \tag{14}$$

where $X := (F, L, V) \in \mathcal{X} := \mathbb{R}^{n_u \times n_y} \times \mathcal{S}^{n_x} \times \mathcal{S}^{n_x}$. We assume that $J : \mathcal{X} \to \mathbb{R}$, $H, G, Y : \mathcal{X} \to \mathcal{S}^{n_x}$ are twice continuously (Frechét–) differentiable matrix functions and the mapping $H(\cdot)$ is only a function in the variables (F, L), i.e., $H_V(X) \equiv 0$. Moreover, for given $X \in \mathcal{F}_s$ we suppose that the linear operators $H_L(X)$ and $G_V(X)$ are invertible, where $\mathcal{F}_s := \{X \in \mathcal{X} \mid Y(X) \succ 0\}$. Obviously, the NSPDs (12) and (13) are in the form of (14). IPCTR is based on the approximate solution of a sequence of matrix equality constraint barrier problems

$$\min \quad \Phi^\mu(X) = J(X) - \mu \log\det(Y(X)) \quad \text{s. t.} \quad H(X) = 0, \quad G(X) = 0, \tag{15}$$

where $\mu > 0$ and $Y(X)$ is (implicitly) assumed to be positive definite. The Lagrangian function associated with (15) is defined by

$$\ell^\mu(X, K) = \Phi^\mu(X) + \langle K_h, H(X)\rangle + \langle K_g, G(X)\rangle$$

where $K := (K_g, K_h) \in \mathcal{S}^n \times \mathcal{S}^n$ are Lagrange multipliers for the equality constraints. The basic IPCTR algorithm combines ideas of (primal) interior point and trust region methods with a modified conjugate gradient (CG) procedure. Please note that a primal–dual method can be used instead of a pure primal method. The primal approach has the advantage that we do not need to compute the dual matrix variables for the nonlinear matrix inequality constraints. In the primal–dual case, the computational complexity of a Newton–type method increases rapidly with the number of the dual matrix variables. In particular, if n_x is large, e. g. $n_x = 4000$, then the dual matrix variable for $Y(X) \preceq 0, Y(X) \in \mathcal{S}^{n_x}$ has several million unknown entries, e. g. $\frac{1}{2} \cdot n_x \cdot (n_x + 1) = 8.002 \cdot 10^6$.

Algorithm 3.1 (IPCTR, see, e.g., [20, 22])
Let $X_0 = (F_0, L_0, V_0)$ with $Y(X_0) \succ 0$ and $\mu_0, \epsilon_0 > 0$ be given. For $j = 0, 1, \ldots$ do:

Find a solution $X_{j+1} = (F_{j+1}, L_{j+1}, V_{j+1}) \in \mathcal{F}_s$ of (15) satisfying

$$||\nabla \ell_F^{\mu_j}(X_{j+1}, K_{j+1})|| + ||H(X_{j+1})|| + ||G(X_{j+1})|| \leq \epsilon_j,$$

where the multipliers $K_{j+1} := (K_h, K_g)_{j+1}$ are the solutions of the adjoint (multiplier) equations $\nabla \ell_L^\mu(X, K_h, K_g) = 0, \nabla \ell_V^\mu(X, K_h, K_g) = 0$; e.g. ,

$$K_g = -(G_V^{-1}(\cdot))^* \nabla \Phi_V^\mu(\cdot), \quad K_h = -(H_L^{-1}(\cdot))^* (\nabla \Phi_L^\mu(\cdot) - G_L^*(\cdot) K_g).$$

Choose $\mu_{j+1} < \mu_j$ and $\epsilon_{j+1} < \epsilon_j$.

In an implementation of IPCTR, we have chosen the parameters μ_j and ϵ_j as stated in [22]. In particular, if the actual barrier parameter $\mu_j < 1$ we set $\mu_{j+1} = \Omega(\mu_j^{\frac{4m}{2m+1}})$, $m \in \mathbb{N}$. This is equivalent to $\mu_{j+1} \geq \mu_j^{\frac{4m}{2m+1}}$, where for related positive quantities α and β, we write $\alpha = \mathcal{O}(\beta)$ if there is a constant $\kappa > 0$ such that $\alpha \geq \kappa\beta$ for all β sufficiently small and $\alpha = \Omega(\beta)$ if $\beta = \mathcal{O}(\alpha)$. Otherwise, we choose $\mu_{j+1} = a\mu_j$, $a \in (0, 1)$. Using this rule, the rate at which the barrier parameter approaches zero can be made as close to quadratic as one desires. The updating rule for the inexact termination criterion is given by $\epsilon_{j+1} = \mathcal{O}(\mu_{j+1}^{\frac{1}{m}})$. In our practical implementation, we choose $m \in \{2, 3, 4, 5\}$. Making standard assumptions on problem (14), it can be proved that any cluster point of the sequence $\{X_j\}_{j \geq 0}$ generated by IPCTR is a KKT point of (14). For the proof we refer to [20, Theorem 3.1]. The tool used in IPCTR for finding a solution of (15) is a tangent space trust region method (see, e.g., [5, 6, 8, 20, 23]). For given X, in this variant the step $\Delta X = (\Delta F, \Delta L, \Delta V) = T(X)\Delta F + N(X)$ is decomposed into the tangential step $T(X)\Delta F$ and the normal step $N(X)$, respectively. Here we define $T(\cdot) = (\mathcal{I}, T_1(\cdot), T_2(\cdot)) \in \mathcal{L}(\mathbb{R}^{n_u \times n_y}, \mathcal{X})$, where $\mathcal{I} : \mathbb{R}^{n_u \times n_y} \to \mathbb{R}^{n_u \times n_y}$ is the identity mapping and T_1, T_2 are given by

$$T_1(\cdot) := -H_L^{-1}(\cdot) H_F(\cdot), \;\; T_2(\cdot) := -G_V^{-1}(\cdot) \left(G_F(\cdot) - G_L(\cdot) H_L^{-1}(\cdot) H_F(\cdot) \right).$$

Moreover, $N(\cdot) = \left(0, -H_L^{-1}(\cdot)H(\cdot), -G_V^{-1}(\cdot)(G(\cdot) - G_L(\cdot)H_L^{-1}(\cdot)H(\cdot))\right) \in \mathcal{X}$, where 0 is the zero matrix. Using [22, Lemma 4.1] the normal step $N(\cdot)$ can be determined as follows: First, compute $(\Delta L^n, \Delta V^n)$ by solving the matrix equations

$$H_L(X)\Delta L^n + H(X) = 0, \quad G_V(X)\Delta V^n + G_L(X)\Delta L^n + G(X) = 0,$$

and second, control the size of $(\Delta L^n, \Delta V^n)$ such that they stay inside the current trust region. In this example, we compute the scalar $\beta \in (0,1]$ by $\beta = 1$ if $||(\Delta L^n, \Delta V^n)|| \leq \omega\delta$, else $\beta = (\omega\delta)/||(\Delta L^n, \Delta V^n)||$ and set $(\Delta L^n, \Delta V^n) = \beta(\Delta L^n, \Delta V^n)$, where $\omega \in (0,1)$ is a given scalar and $\delta > 0$ denotes the current trust region radius. The tangential component depends on ΔF and, thus, if ΔF is known, we can compute $(\Delta L^t, \Delta V^t) = (T_1(\cdot)\Delta F, T_2(\cdot)\Delta F)$ as solutions of two linear matrix equations

$$H_L(X)\Delta L^t + H_F(X)\Delta F = 0, \quad G_V(X)\Delta V^t + G_L(X)\Delta L^t + G_F(X)\Delta F = 0. \quad (16)$$

For computing ΔF we search a solution of the tangential trust region subproblem

$$\begin{aligned} \min \quad & \Psi(\Delta F) = \langle \Delta F, T^*\nabla\Phi_X^\mu + T^*\nabla^2\ell_{XX}^\mu N\rangle + \tfrac{1}{2}\langle \Delta F, T^*\nabla^2\ell_{XX}^\mu T\Delta F\rangle \\ & ||\Delta F|| \leq \delta, \quad Y(X + T(X)\Delta F + \Delta X^n) \succeq (1-\sigma)Y(X), \end{aligned} \quad (17)$$

where $\nabla\Phi_X^\mu = (\nabla\Phi_F^\mu(X), \nabla\Phi_L^\mu(X), \nabla\Phi_V^\mu(X)) \in \mathcal{X}$, $\ell^\mu = \ell^\mu(X, K_g, K_h)$, T and N are the tangential and the normal operator, respectively, $\sigma \in (0,1)$ is given, $\Delta X^n = (0, \Delta L^n, \Delta V^n)$ and $X + T\Delta F + \Delta X^n = (F + \Delta F, L + T_1\Delta F + \Delta L^n, V + T_2\Delta F + \Delta V^n)$. We apply the modified conjugate gradient (CG) algorithm as described in [20, Algorithm 2.1] for finding an approximate solution ΔF of (17). This CG approach has the following properties:

(i) It solves a reduced Newton–like equation in ΔF; i. e. on exit, the solution ΔF of (17) satisfies approximately the equation $\Psi_{\Delta F} = 0$, e. g.

$$T^*(X)\nabla^2\ell_{XX}^\mu(\cdot)T(X)\Delta F = -T^*(X)(\nabla\Phi_X^\mu(X) + \nabla^2\ell_{XX}^\mu(\cdot)N(X)).$$

(ii) During each CG iteration, we compute a maximal scalar $\tau > 0$ such that the matrix inequality constraint in (17) is fulfilled. On exit it is guaranteed that ΔF stays inside the trust region and $X + T(X)\Delta F + \Delta X^n$ satisfies the NSDP constraint in (17).

(iii) In every CG iteration the operator T has to be applied. In particular, for a given conjugate direction δF_{cg}, we solve the first linear matrix equation in (16) for ΔL^t (e. g. $\Delta L^t = T_1(\cdot)\delta F_{cg}$). Then we substitute this solution into the second equation of (16) and solve it for ΔV^t (e. g. $\Delta V^t = T_2(\cdot)\delta F_{cg}$).

(iv) There are different ways in which the CG method can terminate: (a) A direction of negative curvature is encountered in the CG iteration. In this case, we follow this direction until reaching the boundary of the intersection of the trust region and the NSDP–constraints. Then the resulting step is returned as an approximate solution of (17). (b) The CG iterate has stepped outside of the intersection of the trust region and the NSDP–constraints. In this case, we backtrack to this region and return the resulting step as a solution of (17). (c) The algorithm terminates with a pre–specified inexact termination criterion.

The advantages of this strategy are: The CG–loop works only in the space of the F–variable, which is in general much smaller as the abstract state space $\mathcal{S}^n \times \mathcal{S}^n$, where the variables (L, V) lives in. There is no need for evaluating the Hessian of the Lagrangian explicitly. We only need to evaluate it applied to a direction. On exit, it is guaranteed that the matrix inequality is strictly satisfied. For given ΔF, the L– and V–part of the tangential component ΔX^t can be obtained by solving the linear (matrix) equations in (16). Please note, the trust region method in IPCTR uses a non–orthogonal decomposition of the step and the normal step is actually a so–called quasi–normal step. If the operators H_L and G_V are ill–conditioned, such steps can lead to poor performance of the method. In this case, the trust region variant discussed in [8, Section 5.22] can be used alternatively. To keep the quasi–normal step within the trust region the size factor β is introduced. If the operators are ill–conditioned this may lead to a poor descent step compared to Byrd–Omojukun steps, too. Here a simple dogleg modification in the space of L and V could be used to overcome this problem. Finally, as shown in Wächter and Biegler [29], barrier methods using the step to the boundary rule (which is included in (17)) in combination with linearized equality constraints, can fail by "crashing into bounds". Therefore, it seems that a breakdown may occur in IPCTR for some "degenerated" NSDPs. But, we have tested IPCTR extensively on the *COMPl*$_e$*ib* benchmark library [19] which contains actually 171 test examples. For all test runs we never observed a failure of IPCTR. In particular, for almost all *COMPl*$_e$*ib* test examples, IPCTR performs pretty good and very fast. Even if the operators H_L and G_V are ill–conditioned, the performance of IPCTR was quite satisfactory. Moreover, we never observed the Wächter and Biegler "crashing into bounds"–phenomenon during our test runs of IPCTR on *COMPl*$_e$*ib* . A whole convergence analysis of IPCTR is far beyond the scope of this paper. For more algorithmic details and some convergence results, we refer the interested reader to [8], [20] and [22].

4 Numerical experiments

We conducted numerical experiments in computing linear SOF control laws for several discretized parabolic PDE control systems. To clarify our approach let us summarize the algorithmic steps:

1. solve the discrete dynamical system (9) of dimension n_x for a chosen/nominal control u, e.g., for $u = 0$ (uncontrolled dynamics) to get $x(t_j)$, $j = 1, \ldots, n$ for a time grid in $[0, T]$;

2. define w_j, $j = 1, \ldots, 2n$, according to (3) and choose $\mathcal{V}_1$ or $\mathcal{V}_2$ as well as $\Xi = \mathcal{U}$ or $\Xi = \mathcal{W}$ for (5);

3. compute the first ℓ POD basis functions by solving the eigenvalue problem (7) and using (8);

4. apply a Galerkin ansatz for the PDE utilizing the computed ℓ POD basis functions to derive a discrete dynamical system of the type (9), but with dimension $\ell \ll n_x$ (low–dimensional model);

5. neglect the nonlinear part $G(x(t))$ in (9) and solve SOF–$\mathcal{H}_2$ problem (12) to get a linear SOF control law of the form (10), see Section 3;
6. fit this SOF control into the high–dimensional discrete dynamical system (9) to obtain the closed–loop system

$$\begin{aligned} E\dot{x}(t) &= (A + BFC + \delta A)x(t) + G(x(t)) + B_1\tilde{w}(t), \quad x(0) = x_\circ, \\ z(t) &= (C_1 + D_1FC)x(t). \end{aligned}$$

In step 5 we neglect the nonlinear part in (9) and compute the SOF control law for the linear model. Alternatively, we linearize the nonlinear part instead of neglecting $G(x(t))$. In some cases, this could lead to a poor performance of the SOF controller, e. g. if $G(x(t))$ is highly nonlinear. For moderate nonlinear terms, the linear SOF control law is a good feedback control for the nonlinear system, too. For highly nonlinear models, it is likely that such a simple linear SOF controller can not stabilize the unstable nonlinear system. In these cases, a nonlinear feedback should be used.

The computational performance of this method is pretty fast. The main work is the computation of the POD approximation of the large (nonlinear) system. Typically, we reduce the size from several thousand variables to 5–10 variables in the POD model. In this case, the corresponding NSDP (12) is a matrix optimization problem with approximately $25 - 100$ unknowns and, typically, IPCTR computes a (local) solution of the small–sized NSDPs within some seconds on a DELL notebook.

4.1 Example (Linear convection–diffusion model)

The first example is a two dimensional model of a linear parabolic equation with n_u distributed control input functions in the domain $\Omega = [0, a] \times [0, b]$, where $a = 1, b = 1$. The infinite dimensional control problem of the convection–diffusion model is given by

$$\begin{aligned} v_t &= \kappa\Delta v - \varepsilon_1(v_\xi + v_\eta) + \varepsilon_2 v + \textstyle\sum_{i=1}^{n_u} u_i(t)b_i, && \text{in } \Omega, t > 0, \\ v(\xi, \eta; t) &= 0, && \text{on } \partial\Omega, t > 0, \\ v(\xi, \eta, 0) &= v_0(\xi, \eta), && \text{in } \Omega, \end{aligned} \tag{18}$$

for the unknown function $v := v(\xi, \eta; t)$, $(\xi, \eta) \in \Omega$, $t > 0$, where Δ denotes the Laplace operator, $\varepsilon_1, \varepsilon_2 \geq 0$ are given constants, $\partial\Omega$ denotes the boundary of Ω, $\kappa > 0$ is the diffusion coefficient, $b_i, i = 1, \ldots, n_u$ are given shape functions for the control inputs $u_1, \ldots, u_{n_u}$ and $v_0(\cdot)$ is the initial state in Ω at $t = 0$. After a spatial finite difference discretization of (18) we end up with a linear control system of the form (9) with $E = I$, $\delta A \equiv 0$, $G(x(t)) \equiv 0$ and $n_x = 3600$ states. We choose $n_u = 2$ and $b_i = \chi_{\Omega_i^u}$, $i = 1, 2$, where $\chi_{\Omega_i^u}$ denotes the characteristic function on the control input domain $\Omega_i^u \subset \Omega$ of u_i and

$$\Omega_1^u = [0.1, 0.4] \times [0.1, 0.4], \quad \Omega_2^u = [0.6, 0.9] \times [0.7, 0.9].$$

Moreover, we set $n_y = 2$ and measure the state on the observation domains $\Omega_i^y \subset \Omega, i = 1, 2$ of $y(t) = (y_1(t), y_2(t))^T$, where

$$\Omega_1^y = [0.1, 0.4] \times [0.5, 0.7], \quad \Omega_2^y = [0.6, 0.9] \times [0.1, 0.4].$$

Table 1. Parameter for Ex. 4.1

n_x	n_u	n_y	ℓ	κ	c_1	d_1	ε_1	ε_2
3600	2	2	7	0.06119	10	100	0.29555	2.9555

Hence, the data matrices $B \in \mathbb{R}^{n_x \times n_u}$, $C \in \mathbb{R}^{n_y \times n_x}$ only contain zeros and ones with ones at grid points within the control input and observation domains, respectively.

Figure 1. Ex. 4.1 with SOF at $t = 0.8, 2, 4, 8$: POD with $\mathcal{V}_1$, $\Xi = L^2(\Omega)$ (left), $\mathcal{V}_1$, $\Xi = H^1(\Omega)$ (right).

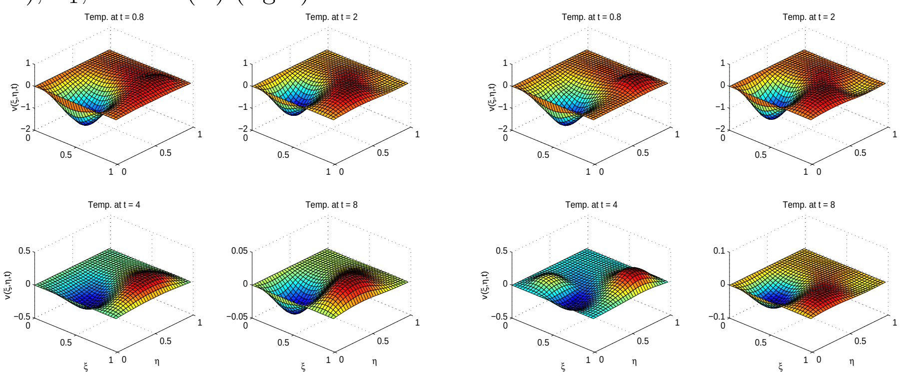

Figure 2. SOF control (10) for Ex. 4.1: POD with $\mathcal{V}_1$, $\Xi = L^2(\Omega)$ (left), $\mathcal{V}_1$, $\Xi = H^1(\Omega)$ (right).

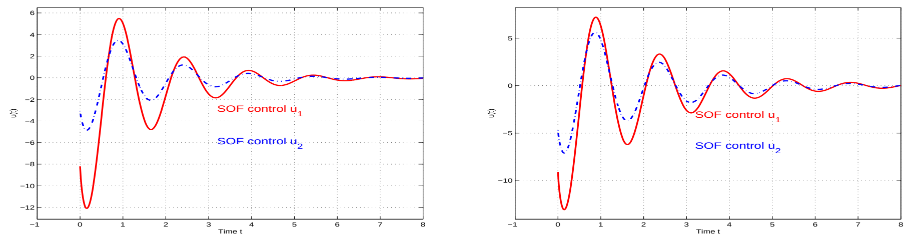

Table 1 lists the parameters that we have used in our numerical experiments. Note, due to the choice of ε_2 (see Table 1), the uncontrolled system is unstable. In example, the real part of the largest eigenvalue of A is positive. Figure 1 shows the state of the linear convection–diffusion model (18) if we use SOF control law computed by IPCTR in combination with POD. We have computed the first $\ell = 7$ POD basis functions utilizing the (discrete) L^2–norm (left) as well as the discrete H^1–norm (right). This figure illustrates that the simple SOF controller stabilizes

Figure 3. Ex. 4.1 with SOF at $t = 0.8, 2, 4, 8$: POD with $\mathcal{V}_2$, $\Xi = L^2(\Omega)$ (left), $\mathcal{V}_2$, $\Xi = H^1(\Omega)$ (right).

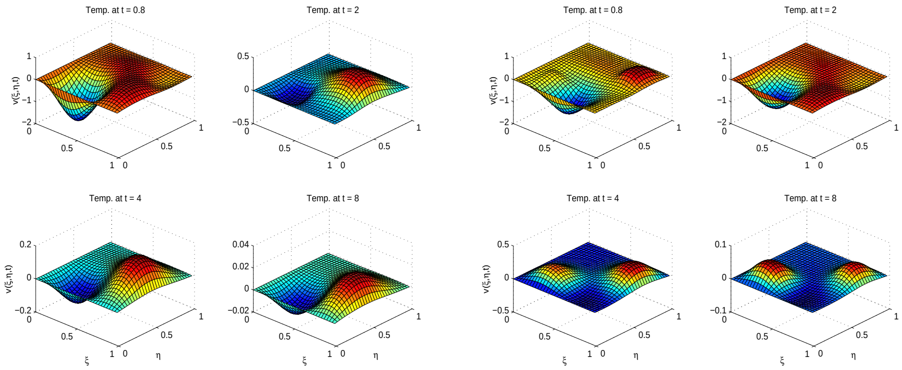

the unstable control system very well. The corresponding controller functions can be found in Figure 2. The plots in Figure 3 shows the dynamical behavior of the controlled model for the choice of a different snapshot ensemble. In particular, for the computation of the POD basis function we only use every 10–th snapshot and include the difference quotients in the snapshot ensemble. The corresponding

Figure 4. SOF control (10) for Ex. 4.1: POD with $\mathcal{V}_2$, $\Xi = L^2(\Omega)$ (left), $\mathcal{V}_2$, $\Xi = H^1(\Omega)$ (right).

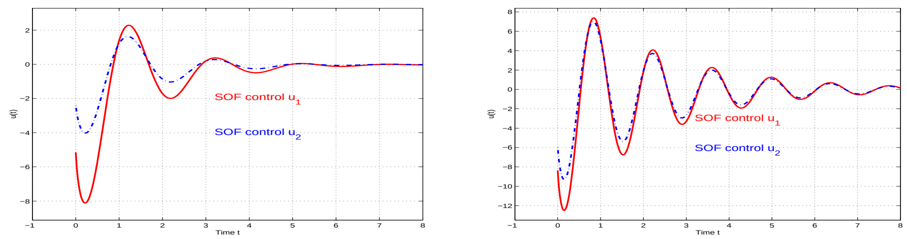

control input functions are illustrated in Figure 4. On the other hand, Figure 5 visualizes the instability of this model. Moreover, Figure 6 illustrates the location of the two sensor (red) and control (green) domains in Ω. It turns out that in case of $\Xi = L^2(\Omega)$ and $\mathcal{V}_2$ the SOF control has the best stability characteristics. For $\Xi = H^1(\Omega)$ we observe that there is no big difference if the time derivatives are included in the snapshots or not.

4.2 Example (Nonlinear unstable heat equation)

Our next example deals with a two dimensional distributed control input model of a nonlinear instable heat equation. In the domain $\Omega = [0, 1] \times [0, 1]$ we consider a initial boundary value problem of this nonlinear reaction–diffusion model for the

Figure 5. Ex. 4.1 with no control at $t = 0.8, 2, 4, 8$.

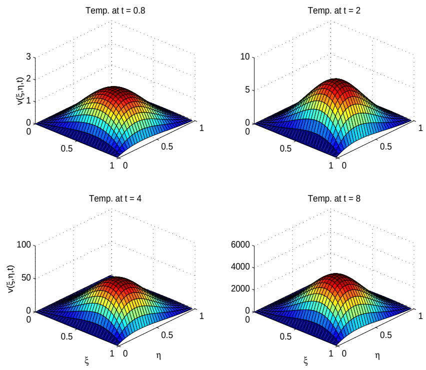

Figure 6. Ex. 4.1: Sensor and control domains.

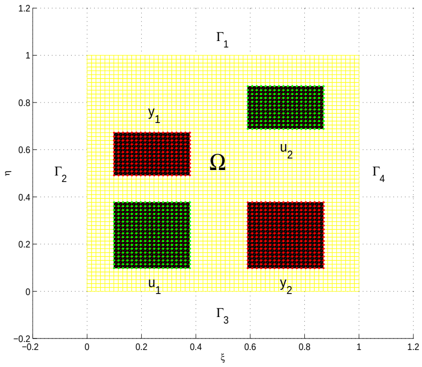

unknown function $v(\xi, \eta; t)$, $(\xi, \eta) \in \Omega$, $t > 0$:

$$\begin{array}{rcll} v_t & = & \kappa \Delta v + \varepsilon_2 v - \varepsilon_1 v^3 + \sum_{i=1}^{n_u} u_i(t) b_i, & \text{in } \Omega, t > 0, \\ v(\xi, \eta; t) & = & 0, & \text{on } \partial\Omega, t > 0, \\ v(\xi, \eta, 0) & = & v_0(\xi, \eta), & \text{in } \Omega, \end{array} \tag{19}$$

where $\varepsilon_1, \varepsilon_2 \geq 0$ are positive constants and the other quantities are defined as in the

Figure 7. Ex. 4.2 with no control at $t = 0.8, 2, 4, 8$.

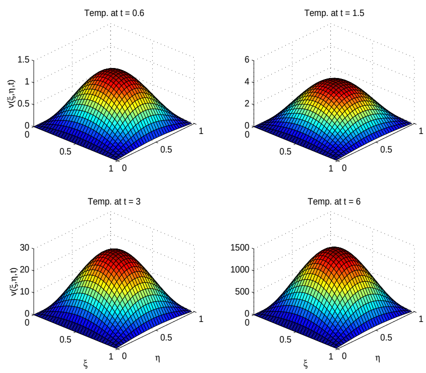

Figure 8. Ex. 4.2: Sensor and control domains.

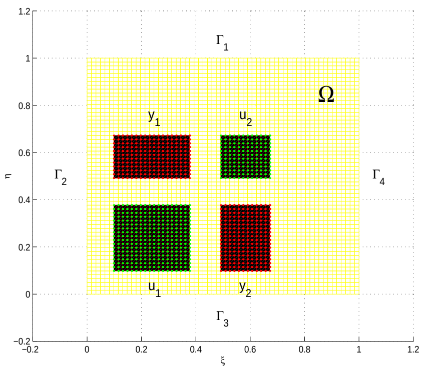

previous example. For $\varepsilon_1 = 0$ and $\varepsilon_2 = 0$, the open loop system of (19) is the heat equation, which is asymptotically stable. However, it is unstable if $\varepsilon_2 > 0$ is large enough even if $\varepsilon_1 = 0$. We use a back–stepping method for the finite difference semi–discretized approximation of (19) (with uniform mesh size $h = 0.01639$ to ensure at least a small error in the spatial approximation) which results in a nonlinear control system of the form (9) with $E = I$, $\delta A \equiv 0$, $G(x(t)) = -\varepsilon_1 x(t)^3$ and $n_x = 3600$ state variables. Moreover, we assume that we have two fixed sensor ($n_y = 2$) and two fixed control ($n_u = 2$) domains located in Ω. In particular, Figure 8 visualizes the

Table 2. Parameter for Ex. 4.2

n_x	n_u	n_y	ℓ	κ	c_1	d_1	ε_1	ε_2
3600	2	2	5	0.06119	100	10	1.0	2.5

Figure 9. Ex. 4.2 with SOF at $t = 0.8, 2, 4, 8$: POD with $\mathcal{V}_1$, $\Xi = L^2(\Omega)$ (left), $\mathcal{V}_1$, $\Xi = H^1(\Omega)$ (right).

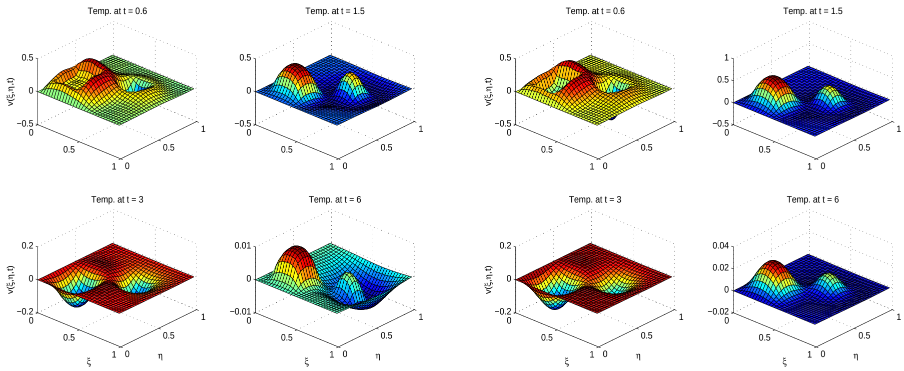

Figure 10. SOF control (10) for Ex. 4.2: POD with $\mathcal{V}_1$, $\Xi = L^2(\Omega)$ (left), $\mathcal{V}_1$, $\Xi = H^1(\Omega)$ (right).

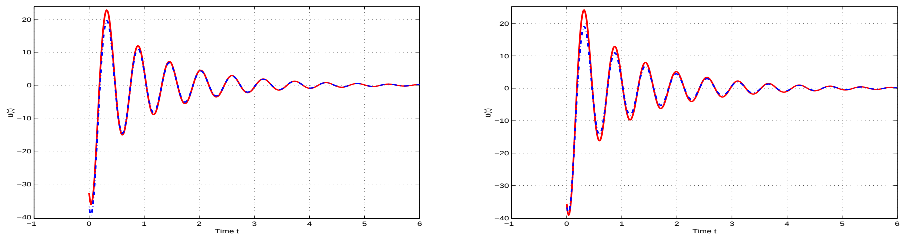

location of the two control (green) and sensor (red) domains in Ω, respectively. The instability of the linear (e.g., $\varepsilon_1 = 0$) uncontrolled model is illustrated in Figure 7. In our numerical experiments for this nonlinear model we have used the parameters in Table 2. For the computation of the low–dimensional POD approximation of the nonlinear model, we use snapshots of the linearized unstable and uncontrolled system as shown in Figure 7. In this case study we have computed the first $\ell = 5$

POD basis functions utilizing the (discrete) L^2–norm as well as the discrete H^1–norm. Figure 9 shows the results of our experiments. Therein, we have plotted the temperature distribution of the nonlinear model (19) if we use the SOF controller computed by IPCTR in combination with POD. At $t = 6$, Figure 9 illustrates that

Figure 11. Ex. 4.2 with SOF at $t = 0.8, 2, 4, 8$: POD with $\mathcal{V}_2$, $\Xi = L^2(\Omega)$ (left), $\mathcal{V}_2$, $\Xi = H^1(\Omega)$ (right).

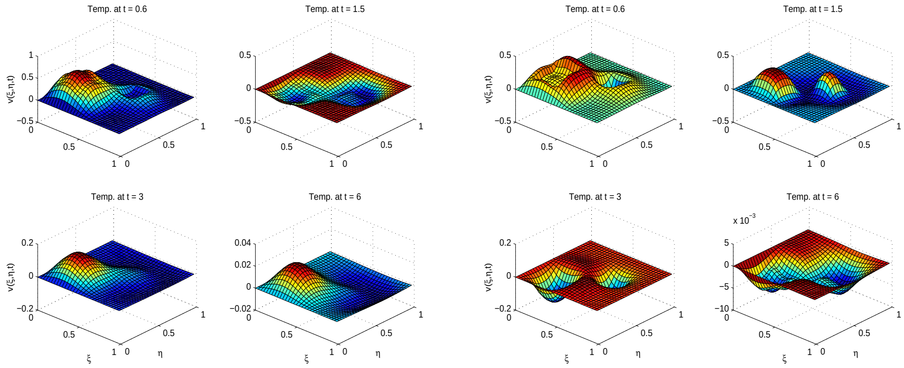

Figure 12. SOF control (10) for Ex. 4.2: POD with $\mathcal{V}_2$, $\Xi = L^2(\Omega)$ (left), $\mathcal{V}_2$, $\Xi = H^1(\Omega)$ (right).

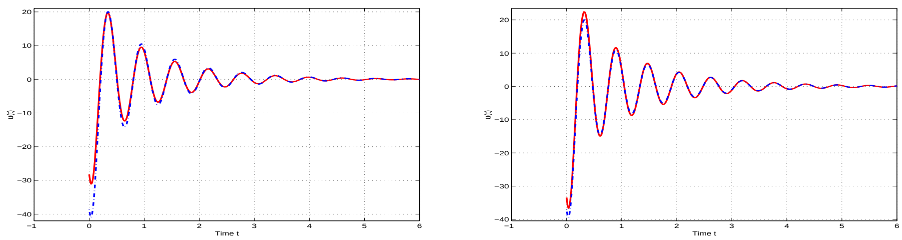

the controlled dynamics are closer to zero with respect to the L^2–norm than the H^1–norm POD approximation. The corresponding optimal output feedback control functions acting on the control domains in Ω can be found in Figure 10. The plots in Figure 11 contain the temperature distributions of the controlled nonlinear model for the choice of a different snapshot ensemble. In particular, for the computation of the POD basis function we only use every 10–th snapshot and include the difference quotients in the snapshot ensemble. In this case, the temperature of the controlled system tends faster to the stable equilibrium state at zero with respect to the H^1–norm and included difference quotient than for all the other POD approximations. In this case, the output feedback control functions are given in Figure 12.

4.3 Example (Modified Burgers' equation)

Now we turn to our third example, where we consider the viscous modified Burgers equation

$$
\begin{aligned}
v_t - \nu v_{\xi\xi} + v v_\xi - \varepsilon v &= 0 && \text{in } Q = (0,T)\times\Omega,\\
\nu v'(t,0) &= 0 && \text{for all } t \in (0,T),\\
\nu v'(t,2\pi) &= u && \text{for all } t \in (0,T),\\
v(0,\xi) &= \sin(\xi) && \text{for all } \xi \in \Omega = (0,2\pi),
\end{aligned}
\tag{20}
$$

where $\nu = 0.5$ denotes a viscosity parameter, $T = 2 > 0$ is the end time, $u \in L^2(0,T)$ is the control input and $\varepsilon = 0.125$. In the context of feedback control for Burgers equation with POD we refer to [2, 16], for instance.

There is only one control input acting on the right-end of the interval Ω. The only measured information available to this control is the state at time $t \in (0,T)$ at $\xi = 2\pi$, i.e.,

$$
y(t) = v(t,2\pi) \quad \text{for all } t \in (0,T). \tag{21}
$$

As in the two previous examples, we can express (20)–(21) by a dynamical system in an appropriate (infinite–dimensional) state space.

Figure 13. Ex. 4.3 with no control.

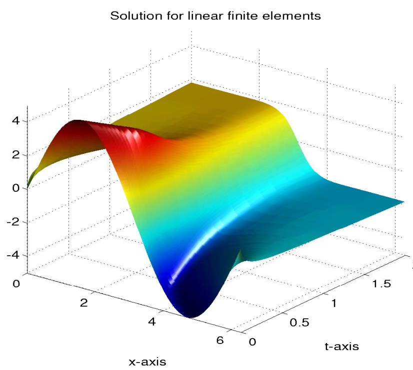

Figure 14. Decay rates: $t \to |v(t,2\pi)|$

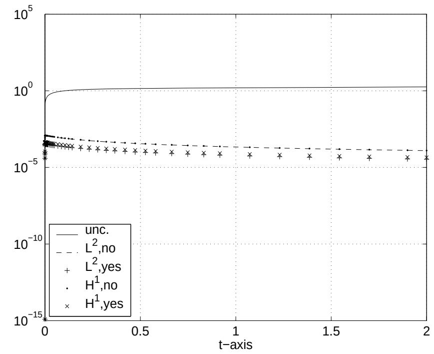

The goal of our optimal control problem is to compute a SOF control law to track the system to zero, i.e., to minimize the cost

$$
J(v,u) = \frac{1}{2}\int_0^T \int_\Omega |v(t,\xi)|^2 + |v_\xi(t,\xi)|^2 \,\mathrm{d}\xi\mathrm{d}t + \frac{\beta}{2}\int_0^T |u(t)|^2 \,\mathrm{d}t,
$$

where $\beta = 10^{-6}$ is a fixed regularization parameter. Notice, that for every $t \in (0,T)$ there is only one observation and one control point. Thus, the control influence is not too big and the SOF control law F is a real number.

For the finite element discretization we utilize the software Femlab, Version 2.2, where we took linear Lagrange elements with 1258 degrees of freedom. The uncontrolled dynamics are presented in Figure 13.

Table 3. Parameters for Ex. 4.2

	$\mathcal{E}(3)$	F	$J(v,u)$	$\int_0^T \lvert v(t,2\pi)\rvert\,\mathrm{d}t$
$\Xi = L^2$, $\mathcal{V}_1$	99.95 %	-2060.07	69.08	0.0006
$\Xi = H^1$, $\mathcal{V}_2$	92.37 %	-7536.10	69.12	0.0000
$\Xi = L^2$, $\mathcal{V}_1$	99.38 %	-2017.68	69.09	0.0006
$\Xi = H^1$, $\mathcal{V}_2$	79.39 %	-5657.58	69.06	0.0002
$u = 0$	—	—	73.34	3.0109

Utilizing $\ell = 3$ POD basis function we compute the SOF control law (10) and solve the closed loop dynamics. Including more information into the snapshot set, e.g., difference quotient or gradient norms, the value of $\mathcal{E}(\ell)$ decreases. In particular, for the choices $\Xi = H^1(\Omega)$ and $\mathcal{V}_2$ we have $\mathcal{E}(3) < 80$ %. However, the damping of $t \mapsto v(t, 2\pi)$ is better than for the choice $\mathcal{V}_1$, independent of Ξ, compare Figure 14. Also the values of the SOF control law are quite different. The values for $\mathcal{V}_1$, i.e., without including the discrete time derivatives, are of the same magnitude, whereas F is much greater if we take the ensemble $\mathcal{V}_2$. Due to the soft control input the cost is only reduced by about 6 %.

5 Conclusions

In this article we consider the SOF problem for PDE constrained control problems in combination with the POD reduction method for deriving a low dimensional control system and the interior point trust region algorithm for solving the corresponding low dimensional NSDP. The SOF control law can be constructed from the solution of the low dimensional NSDP. In our numerical examples, we observe that this SOF can be used for controlling the large dimensional PDE system. In particular, it turns out that including the difference quotients into the POD snapshot ensemble leads to better stability properties of the computed SOF control laws.

Bibliography

[1] A. Adrover and M. Giona. Model reduction of PDE models by means of snapshot archetypes. *Physica D*, 182:23–45, 2003.

[2] J. A. Atwell, J. T. Borggaard, and B. B. King. Reduced Order Controllers for Burgers' Equation with a Nonlinear Observer. *Int. J. Appl. Math. Comput. Sci.*, 11(6):1311–1330, 2001.

[3] D. S. Bernstein and W. M. Haddad. LQG control with an $\mathcal{H}_\infty$ performance bound: a Riccati equation approach. *IEEE Transactions on Automatic Control*, 34:293–305, 1989.

[4] S. P. Boyd, L. E. Ghaoui, E. Feron, and V. Balakrishnan. Linear matrix inequalities in system and control theory. Vol. 15 of *SIAM Studies in Applied Mathematics*, SIAM, Philadelphia, 1994.

[5] R. H. Byrd. Robust trust region methods for nonlinearly constrained optimization. Presented at SIAM Conference on Optimization, Houston, 1987.

[6] A. R. Conn, N. I. M. Gould, and P. Toint. *Trust–region methods.* MPS–SIAM Series on Optimization, SIAM publications, Philadelphia, PA, USA, 2000.

[7] R. F. Curtain and H. J. Zwart. *An introduction to infinite dimensional linear system theory.* Vol. 21 of *Texts in Applied Mathematics*, Springer–Verlag, New York, 1995.

[8] J. E. Dennis, M. Heinkenschloss, and L. N. Vicente. Trust–region interior–point SQP algorithms for a class of nonlinear programming problems. *SIAM Journal on Control and Optimization*, 36:1750–1794, 1998.

[9] M. Hinze and S. Volkwein. Proper orthogonal decomposition surrogate models for nonlinear dynamical systems: error estimates and suboptimal control. Sonderforschungsbereich *Elektromagnetische Strömungsbeeinflussung in Metallurgie, Kristallzüchtung und Elektrochemie*, Report No. 27–2004, to appear in Lecture Notes in Computational Science and Engineering, Vol. 45, 2005.

[10] C. W. J. Hol, C. W. Scherer, E. G. van der Meché, and O. H. Bosgra. *A nonlinear SDP approach to fixed–order controller synthesis and comparison with two other methods applied to an active suspension system.* *European Journal of Control*, 9, 2003.

[11] P. Holmes, J. L. Lumley, and G. Berkooz. *Turbulence, Coherent Structuress, Dynamical Systems and Symmetry.* Cambridge Monographs on Mechanics. Cambridge University Press, 1996.

[12] T. Iwasaki, R. E. Skelton, and J. C. Geromel. Linear quadratic suboptimal control with static output feedback. *Systems & Control Letters*, 23:421–430, 1994.

[13] P. P. Khargonekar and M. A. Rotea. Mixed $\mathcal{H}_2/\mathcal{H}_\infty$ control: A convex optimization approach. *IEEE Transactions on Automatic Control*, 36:824–837, 1991.

[14] K. Kunisch and S. Volkwein. Control of Burgers' equation by a reduced order approach using proper orthogonal decomposition. *J. Optimization Theory and Applications*, 102:345–371, 1999.

[15] K. Kunisch and S. Volkwein. Galerkin proper orthogonal decomposition methods for a general equation in fluid dynamics. *SIAM Journal on Numerical Analysis*, 40:492–515, 2002.

[16] K. Kunisch, S. Volkwein, and L. Xie. HJB-POD based feedback design for the optimal control of evolution problems. To appear in *SIAM Journal on Applied Dynamical Systems*.

[17] F. Leibfritz. *Static Output Feedback Design Problems*. Shaker Verlag, Aachen, Germany, ISBN 3-8265-4203-7, 1998.

[18] F. Leibfritz. A LMI–based algorithm for designing suboptimal static $\mathcal{H}_2/\mathcal{H}_\infty$ output feedback controllers. *SIAM Journal on Control and Optimization*, 39:1711–1735, 2001.

[19] F. Leibfritz. *COMPl$_e$ib*: *CO*nstrained *M*atrix–optimization *P*roblem *lib*rary – a collection of test examples for nonlinear semidefinite programs, control system design and related problems. Tech. report, Universität Trier, 2003. To appear in Special issue of *European Journal of Control* on *Linear Matrix Inequalities in Control*, 2005

[20] F. Leibfritz and E. M. E. Mostafa. An interior point constrained trust region method for a special class of nonlinear semi–definite programming problems. *SIAM Journal on Optimization*, 12:1048-1074, 2002.

[21] F. Leibfritz and E. M. E. Mostafa. Trust region methods for solving the optimal output feedback design problem.: *International Journal of Control*, 76:501-519, 2003.

[22] F. Leibfritz and S. Volkwein. Reduced order output feedback control design for PDE systems using proper orthogonal decomposition and nonlinear semidefinite programming. To appear in Special issue of *Linear Algebra and its Applications* on Order Reduction of Large-Scale Systems, 2005.

[23] E. O. Omojokun. *Trust region strategies for optimization with nonlinear equality and inequality constraints.* Ph. D. thesis, University of Colorado, Boulder, 1989.

[24] A. Pazy. *Semigoups of Linear Operators and Applications to Partial Differential Equations.* Springer-Verlag, New York, 1983.

[25] L. Sirovich. Turbulence and the dynamics of coherent structures. Parts I–III. *Quarterly of Applied Mathematics, XLV*, pages 561-590, 1987.

[26] V. L. Syrmos, C. T. Abdallah, P. Dorato, and K. Grigoriadis. Static output feedback – A survey. *Automatica*, 33:125–137, 1997.

[27] S. Volkwein. Optimal control of a phase-field model using the proper orthogonal decomposition. *Zeitschrift für Angewandte Mathematik und Mechanik*, 81:83–97, 2001.

[28] S. Volkwein. Interpretation of proper orthogonal decomposition as singular value decomposition and HJB-based feedback design Proceedings of the *16th International Symposium on Mathematical Theory of Networks and Systems (MTNS)*, Leuven, Belgien, Juli 5–9, 2004.

[29] A. Wächter, and L. T. Biegler. Failure of global convergence for a class of interior point methods for nonlinear programming. *Mathematical Programming, Series A*, 88:565–574, 2000.

[30] K. Zhou, J. C. Doyle, and K. Glover. *Robust and optimal control.* Prentice Hall, Upper Saddle River, New Jersey, 1996.